THE EFFECT OF CONSTRAINT ON THE FRACTURE TOUGHNESS OF ADHESIVELY BONDED JOINTS

V. Cooper, A. Ivankovic, A. Karac, N. Murphy
School of Electrical, Electronic and Mechanical Engineering, University College Dublin, Ireland.
vincent.cooper@ucd.ie

Introduction

Although many testing methods and procedures have been standardized and used to characterize adhesive bond toughness, the accurate transfer of laboratory results to complex structures remains questionable. The difficulty arises from the existence of strong bond-line thickness effects on the fracture toughness [1]. We aim to address this problem by examining the level of constraint within the bond-line and hence its effects on the global bond toughness. The thickness and width of the adhesive layer affects the stress and strain distribution in the adhesive. For example, a change of the adhesive layer thickness can cause a transition from small-scale yielding (SSY) conditions within the adhesive to fully plastic conditions [2-4].

The current work examines the fracture behaviour of adhesively bonded joints by conducting a series of low rate tapered double cantilever beam (TDCB) tests with various bond gap thicknesses. The dependence of the adhesive fracture energy, G_{IC}, for a crack propagating cohesively through the adhesive layer upon the thickness and width of the joint is investigated. A single part, nano-rubber toughened, structural epoxy adhesive was used throughout this research. Tests were carried out using two different TDCB setups: *(i)* Steel substrates of 25.4mm width (ASTM D3433) [5] and *(ii)* 10mm wide aluminium 2014 substrates following the BS2001:7991 testing protocol [6].

In order to accurately calculate the fracture toughness, numerical modelling of the TDCB experiments was performed using the finite-volume (FV) approach with a Dugdale shape traction-separation law. Numerical results were compared with experimentally recorded load-displacement and crack-length data. Also, the mean hydrostatic stress (σ_{hyd}) across the crack front is numerically quantified for various bond thicknesses prior to crack initiation. This is used as an estimate of the geometric constraint, i.e. stress tri-axiality. Numerical results indicate that the crack tip stress field is affected by the constraint and hence bond thickness.

In addition, attempts are made to relate the microstructural features on the fracture surfaces with the constraint level and fracture toughness. Higher level of constraint promotes voiding (debonding) of rubber-particles in the local damage region in front of the crack, but it also restricts global plastic deformation of the adhesive.

Materials and Experimental Procedures

The TDCB configuration is used to measure the mode I adhesive fracture energy. As explained above, tests were carried out using two different TDCB setups (Figure 1):

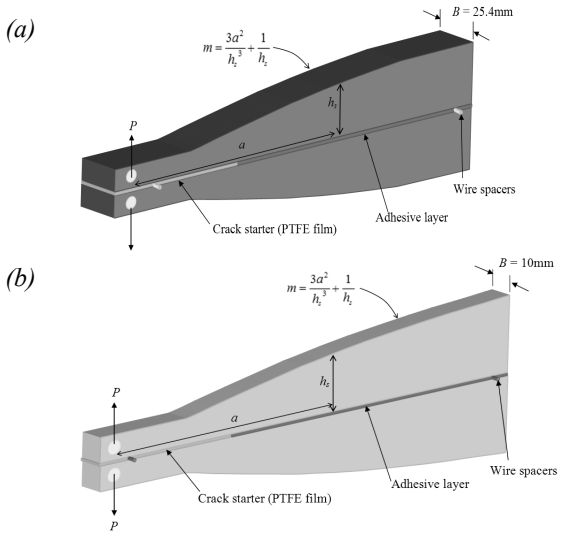

Figure 1: Illustration of the TDCB test specimens: *(a)* 25.4mm wide steel substrate joint and *(b)* the 10mm wide aluminium substrate joint.

The adhesive used is a single part, hot cured structural epoxy adhesive (Henkel 3019-98) containing the following toughening agents - two core shell particle grades and one liquid co-toughener. Two substrate materials are used: *(i)* Aluminium 2014 - a high yield strength alloy which is widely used in automotive applications and *(ii)* Steel EN24T - a high quality, high strength, alloy steel. Uniaxial tensile tests were conducted to obtain the mechanical properties of both the substrate materials and the adhesive. Results of the tests conducted at the strain rate $6x10^{-5}s^{-1}$ (gauge length = 40mm, crosshead speed = 0.1mm/min) are given in the table below.

Table 1. Room temperature tensile properties of aluminium, steel and adhesive at strain rate $6x10^{-5}s^{-1}$.

	E [GPa]	UTS [MPa]	σ_{yield} [MPa]
Al 2014	*72.4*	*430*	*290*
Steel EN24T	*190*	*850*	*654*
Henkel 3019-98	*1.9*	*36.7*	*26*

The bond thickness was set using stainless steel wire spacers. A 12 μm thick film of PTFE was inserted at one end to act as a crack starter as specified in the protocol. The specimens were placed in a jig that maintained alignment, and a slight compressive load was applied. The samples were cured at 180°C for 30min. The tests were carried out at room temperature and records of the load and the displacement at different increments of the crack length

were obtained. At least three repeats for each joint system were tested.

Experimental Results

TDCB testing was carried out at various bond gap thicknesses between 0.4mm and 2.5mm. An increase of G_{IC} with bond gap thickness was observed and a comparison of both sets of data is shown in Figure 2. Steady state crack growth behaviour was observed in all tests. The average fracture energy was calculated using the Corrected Beam Theory approach:

$$G_{CBT} = \frac{4P^2 m}{Eb^2}\left(1 + 0.43\left(\frac{3}{ma}\right)^{1/3}\right) \quad (1)$$

where, P is the mean load during crack propagation, m geometry factor, E Young's modulus of substrate, b width of the beam, and a crack length.

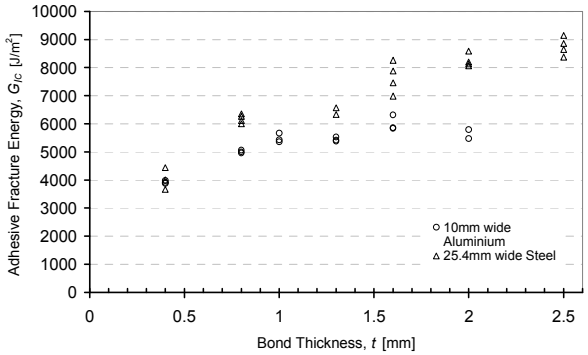

Figure 2: Adhesive fracture toughness as a function of the bond thickness for both TDCB geometries.

For tests with bond thickness less than 1mm, mode I cohesive failure was observed. However when the bond gap thickness was increased above 1mm, a change in the crack behaviour was observed. A slanted fracture gradually developed along the specimen. A local mode III loading was introduced forcing the fracture to change from plane cohesive mode I to slant mixed mode I and III fracture. The transition from cohesive to slant fracture in Aluminum substrate TDCB specimens is illustrated in Figure 3.

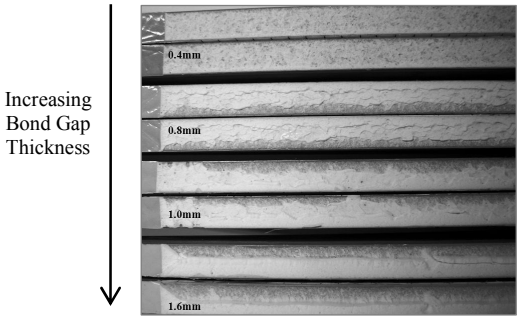

Figure 3: Fracture surfaces illustrating transition to slant fracture on aluminium TDCB specimens.

Side-grooves were introduced to remove the stress free zone on the edge of the adhesive layer to help eliminate the slant fracture (see Figure 4). The grooves were machined on both sides of the specimen to ensure symmetrical deformation.

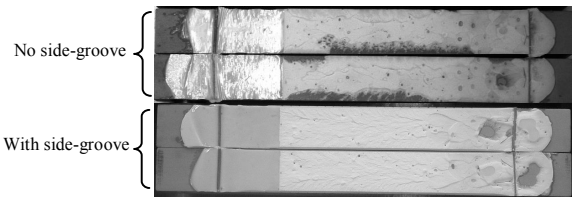

Figure 4: The effect of side grooves on the fracture surface appearance for a 2mm bond thickness case.

FV Modelling

Numerical modelling of both TDCB tests (BS 10mm wide and ASTM 25.4mm wide) was performed using the FV method (OpenFOAM - version 1.3 [7]). The cohesive zone model (CZM) was defined using a two-parameter Dugdale model, with parameters being the adhesive fracture energy G_{IC} and the maximum cohesive stress, σ_{max} = UTS = 36.7MPa. A 2D illustration of the BS 10mm wide mesh used is shown in Figure 5.

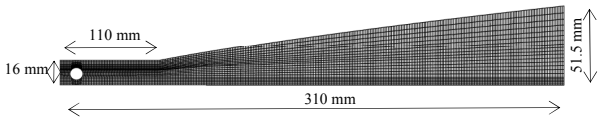

Figure 5: FV representation of the 10mm wide TDCB geometry.

In order to choose the accurate value of G_{IC}, a numerical calibration was undertaken. The value of G_{IC} which gave the best numerical prediction of experimental results (force-displacement and crack length-displacement) was selected. Figure 6 illustrates numerical (elastic-plastic) calibration of G_{IC} for a 10mm wide, 0.4mm bond thickness TDCB experiment.

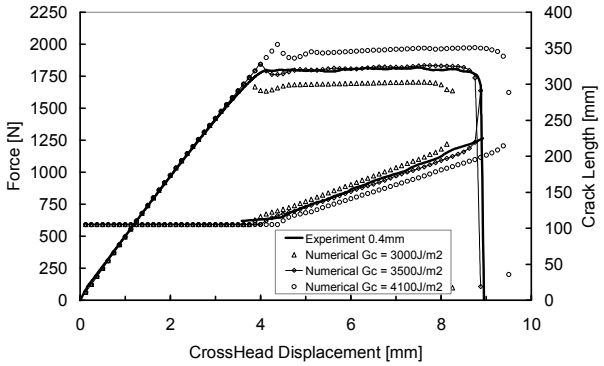

Figure 6: Comparison of numerical and experimental (BS TDCB) results obtained at 0.5mm/min for different G_{IC} values. Best fit: G_{IC} = 3500J/m^2, σ_{max} = 36.7MPa (UTS).

The variation of hydrostatic stress along the crack front for ASTM TDCB specimens with various bond-line thicknesses is presented in Figure 7.

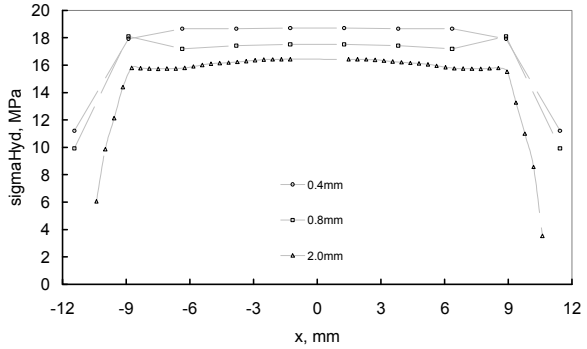

Figure 7: Hydrostatic stress distribution across 25.4mm adhesive bond for various bond gap thicknesses.

A study was carried out to numerically quantify mean hydrostatic stress across the crack front prior to crack initiation. σ_{hyd} is used as an estimate of the geometric constraint and a relationship with G_{IC} is shown in Figure 8.

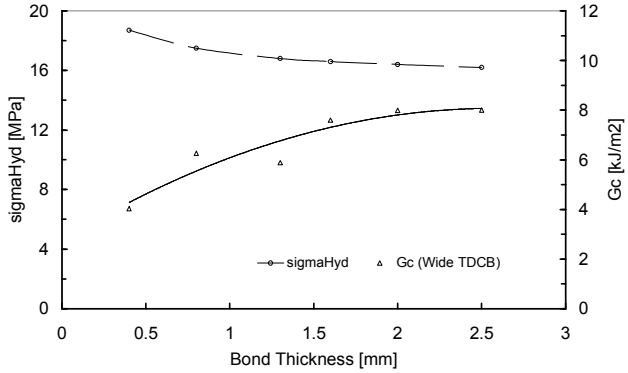

Figure 8: Mean hydrostatic stress and adhesive fracture energy as a function of bond gap thickness.

Microscopy

A detailed analysis of the fracture surfaces, using field emission gun scanning electron microscopy (FEG-SEM) revealed variations of the microstructural features within the adhesive (Figure 9). By analysing the density and size of voids on the fracture surfaces we aim to explain the source of dependency of G_{IC} with constraint (i.e. bond thickness and width), hence verifying the numerical results.

Conclusions and Future Work

- A strong dependency of G_{IC} on bond thickness and width was observed.
- A variation of constraint level for various bond thicknesses was found and an attempt was made to relate G_{IC} with constraint level.
- SEM images show evidence of debonded micro and nano particles from the bulk adhesive, but no cavitation of nanoparticles. These features will be used to bridge the micro and macro scales.

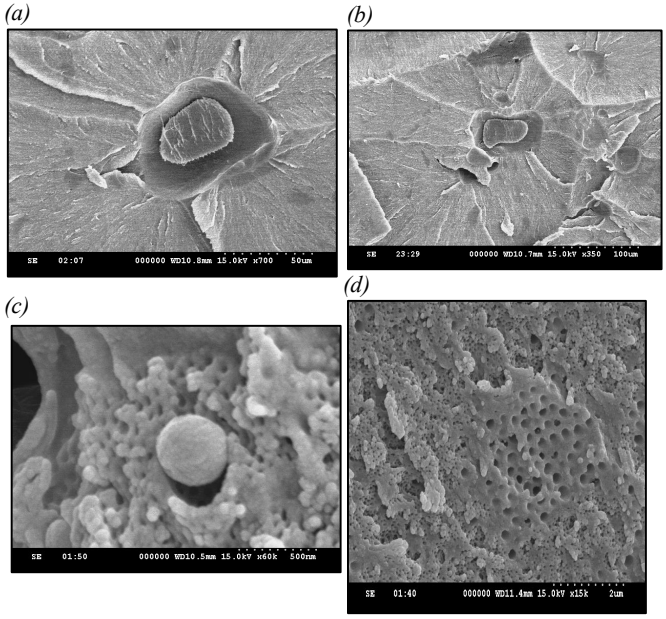

Figure 9: FEG-SEM images of a 2mm bond thickness fracture surface showing - *(a)*, *(b)* liquid co-toughener (rubber pools) and *(c), (d)* core shell particles.

Acknowledgments

The author wishes to acknowledge the funding and support received from Henkel Loctite Ireland and The Irish Research Council for Science Engineering and Technology (IRCSET). The support and help of Dr. Zeljko Tukovic is also greatly appreciated.

References

1. T. Pardoen, T. Ferracin, C.M. Landis, and F. Delannay. Constraint effects in adhesive joint fracture. *Journal of the Mech. and Physics of Solids*, 53, 2005, pp 1951-1983.
2. H. Chai, Deformation and fracture of particulate epoxy in adhesive bonds. *Acta Metall. Mater.,* 43, 1995, pp 163–172.
3. A.J. Kinloch and S.J. Shaw, The Fracture Resistance of a Toughened Epoxy Adhesive, *J. Adhes*., 1981, 12, pp. 59–77.
4. V. Tvergaard, J.W. Hutchinson, Toughness of an interface along a thin ductile layer joining elastic solids. *Philos. Mag.,* 1994, A 70, pp 641–656.
5. ASTM D3433-99, Standard Test Method for Fracture Strength in Cleavage of Adhesives in Bonded Metal Joints.
6. B.R.K. Blackman, A.J. Kinloch, Determination of the mode I adhesive fracture energy, G_{IC}, of structural adhesives using the Double Cantilever Beam (DCB) and the Tapered Double Cantilever Beam (TDCB) Specimens. *ESIS TC4 Protocol 2000* and British Standard BS 7991-2001.
7. Website address: www.openfoam.com